Conservative Solitons and Reversibility in Time Delayed Systems

T. G. Seidel,[1,2] S. V. Gurevich,[2] and J. Javaloyes[1]

[1]Departament de Física and Institute of Applied Computing and Community Code (IAC-3),Universitat de les Illes Baleares, C/Valldemossa km 7.5, 07122 Mallorca, Spain

[2]Institute for Theoretical Physics, University of Münster, Wilhelm-Klemm-Straße 9 and Center for Nonlinear Science (CeNoS), University of Münster, Corrensstraße 2, D-48149 Münster, Germany

(Received 10 September 2021; revised 25 November 2021; accepted 24 January 2022; published 22 February 2022)

Time delayed dynamical systems have proven to be a fertile framework for the study of physical phenomena. In natural sciences, their uses have been limited to the study of dissipative dynamics. In this Letter, we demonstrate the existence of nonlinear reversible conservative time delayed systems. We consider the example of a dispersive microcavity containing a Kerr medium coupled to a distant external mirror. At low energies and in the long delay limit, a multiscale analysis shows the equivalence with the nonlinear Schrödinger equation. We unveil some of the symmetries and conserved quantities, as well as bright temporal solitons. While elastic collisions occur for shallow wave packets, we observe the lack of integrability at higher energies. We recover the Lugiato-Lefever equation in the weakly dissipative regime.

DOI: 10.1103/PhysRevLett.128.083901

Conservative dynamical systems are test benches for nonlinear dynamics. During the second half of the twentieth century, solitary wave solutions of the Korteweg–de Vries and of the nonlinear Schrödinger (NLS) equations sparked a revolution that gave rise to a plethora of works in natural sciences. Conservative solitons can be observed in a variety of fields including fiber optics [1,2], hydrodynamics [3–5], Bose-Einstein condensates [6], and plasmas [7]. In optics, the NLS equation describes the light propagation under the combined action of chromatic dispersion and an intensity dependent refractive index, the so-called Kerr effect. The interplay between these two effects governs the emergence of bright and dark conservative solitons, that possess, in addition, the integrability property [8]. In practice, higher-order nonlinear, dispersive, and especially dissipative effects perturb this ideal picture. However, conservative systems provide for a firm theoretical basis. For instance, weakly dissipative solitons can successfully be understood as perturbed conservative objects. Irreversible processes such as gain and dissipation drive the evolution of the soliton parameters like, e.g., the energy or the momentum, toward an attractor [9–11].

On the other hand, many complex systems ranging from biology to economy can be successfully modeled by time delayed systems (TDSs), see [12,13] for reviews. In the limit of long delays, TDSs are akin, at least in their complexity, to one-dimensional spatially extended systems [14,15]. There, it was shown that the temporal dynamics of TDSs can be mapped onto a two-dimensional representation. This idea was later generalized to multiple, hierarchically long time delays, leading to multidimensional spatially extended systems [16] and the observation of spirals and defect turbulence. This formal correspondence enables a direct interpretation of purely temporal phenomena in terms of diffusive, dissipative spatiotemporal dynamics. Fronts, dissipative solitons, spatiotemporal intermittency and defects, coarsening, and concepts like Eckhaus instability or chimera states can be observed in TDSs [13,17–24]. More recently, it was shown [25] that considering a more general class of singularly perturbed TDSs allows to cancel this generic diffusive behavior which leads to a dispersive response and a purely imaginary eigenvalue spectrum, typical of reversible systems. In addition, some nondissipative properties of functional and neutral TDSs have been studied by the mathematical community, see, e.g., [26–28]. In this Letter, we provide the physical description of a photonic system modeled by a nonlinear, time-reversible, conservative TDS. Moreover, we demonstrate the existence of conservative solitons in TDSs.

We consider a microcavity containing a nonlinear Kerr medium coupled to an external mirror as depicted in Fig. 1(a). Our modeling approach follows the method developed in [25,29–34]. The dynamical model for the slowly varying electromagnetic field envelopes in the microcavity E and the external cavity Y reads

$$\dot{E} = (-1 + i|E|^2)E + hY, \tag{1}$$

$$Y = r_e e^{i\varphi}[E(t-\tau) - Y(t-\tau)]. \tag{2}$$

The microcavity output $O = E - Y$ is the combination of the intracavity photons transmitted by the microcavity and those reflected. The output field is reinjected after a round-trip τ with the attenuation and phase shift factor $r_e e^{i\varphi}$ yielding the coupling between the fields E and Y in Eq. (2). The latter equation does not contain any time derivative and it is

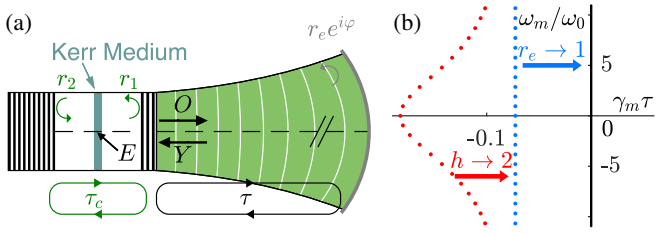

FIG. 1. (a) A schematic of a microcavity with round-trip time τ_c enclosed by two distributed Bragg mirrors with reflectivities $r_{1,2}$. It is coupled to a long external cavity with round-trip time τ which is closed by a mirror with reflectivity r_e. E is the sum of the forward and backward propagating fields that interfere upon the Kerr medium while Y is the field impinging upon the top mirror. (b) The eigenvalue spectrum Eqs. (3) and (4) for different values of h and r_e. For $h < 2$ and $r_e < 1$ (red dots) the spectrum resembles an inverted parabola. When $h \to 2$ (blue dots) it flattens as $\gamma_m\tau = \ln r_e$. For $r_e \to 1$, the spectrum converges to the imaginary axis.

therefore called a delay algebraic equation. This formalism allows us to take into account all the multiple reflections in the external cavity. Note that for $r_e \ll 1$, the infinite hierarchy generated in Eq. (2) could be truncated, leading to an optical feedback term as in the Lang-Kobayashi model [35]. However, in the good cavity limit ($r_e \to 1$), the multiple reflections should be conserved. For a perfectly lossless bottom mirror $|r_2| = 1$ the coupling efficiency parameter is $h = 2$, which corresponds to the Gires-Tournois interferometer regime [36]. Second- and third-order dispersion are naturally captured by Eqs. (1) and (2) as was shown in [25].

Due to the time-delay, the system composed of Eqs. (1) and (2) possesses infinitely many degrees of freedom and its eigenvalue spectrum is a countably infinite set. In the long delay limit $\tau \to \infty$ the spectrum becomes pseudocontinuous [37] and the real part γ_m of the eigenvalues $\lambda_m = \gamma_m + i\omega_m$, obtained around the $(E, Y) = (0, 0)$ solution, can be expressed as a function of its imaginary part ω_m as [25]

$$\gamma_m\tau = \ln r_e + \frac{h-2}{1+\omega_m^2} + \mathcal{O}\left(\frac{1}{\tau}\right), \tag{3}$$

$$\omega_m\tau = 2\pi m + \frac{h-2}{1+\omega_m^2}\omega_m - 2\arctan\omega_m + \mathcal{O}\left(\frac{1}{\tau}\right), \tag{4}$$

with $m \in \mathbb{Z}$, see the red dots in Fig. 1(b). Note that for $h = 2$ the real part γ_m does not depend on ω_m yielding a vertical, yet lossy, spectrum which is shifted from zero by $\ln(r_e)/\tau$ (blue dots). In what follows we consider the lossless cavity limit that corresponds to $(r_e, h) = (1, 2)$ and where λ_m converges toward the unitary spectrum presented in solid black in Fig. 1(b).

In itself, a unitary spectrum is rather surprising in the context of TDSs since it implies the possibility to integrate backward in time without any difficulty. This statement is incompatible with the dynamics of the most widespread TDSs that are based upon delay *differential* equations (DDEs). The latter take the following form

$$\dot{v} = f[v(t), v(t-\tau)], \tag{5}$$

with v a state variable vector. The so-called method of steps [28] implies that an initial condition $\phi(t)$ must be given over an interval of duration τ in order to perform the forward integration over a time τ. Then, this newly propagated segment can be reused as a new initial condition in order to perform the next step. That is, if $\phi(t)$ is a C^p function, *integrating* this function over n steps results in a smoother C^{p+n} profile. Conversely, a C^p initial condition can only be integrated backward during p steps before potentially reaching a discontinuity. All the models based upon DDEs suffer from this difficulty, even in photonics where the latter are based upon the *reversible* Maxwell equations; the approximations made during their derivation [38] set limits over their time-reversed evolution. We note, however, that the delay algebraic model given by Eqs. (1) and (2) or in [25,29–34] do not suffer from this difficulty. This can be understood by combining Eq. (1) with itself evaluated at $t - \tau$ and using Eq. (2) to eliminate the external field Y. Noting $E_\tau \equiv E(t-\tau)$ we obtain

$$E + \dot{E} - i|E|^2E = (E_\tau - \dot{E}_\tau + i|E_\tau|^2E_\tau)e^{i\varphi}. \tag{6}$$

Equation (6) is a neutral delay differential equation (NDDE) where both the delayed value of the field E_τ and its derivative $\dot{E}_\tau$ appear. Since the right hand side of Eq. (6) contains $\dot{E}_\tau$, at each step, the initial condition is both derived and integrated. One understands intuitively that, at variance with DDEs, a C^p initial condition remains C^p and that forward and backward integration do not create asymmetry in the smoothness of the solution profile. Following Kamenskii's classification [28], Eq. (6) is an example of a bilateral NDDE as it preserves its type under time inversion. The general theory of these equations appears to be rich and has not been fully developed yet.

From Eq. (6), the associated linear evolution operator φ_τ propagating the field over a step reads

$$\varphi_\tau : E(t) = \left(1 + \frac{d}{dt}\right)^{-1}\left(1 - \frac{d}{dt}\right)e^{i\varphi}E(t-\tau),$$

while the adjoint operator $\varphi_\tau^\dagger$ is defined as

$$\varphi_\tau^\dagger : W(t) = \left(1 - \frac{d}{dt}\right)^{-1}\left(1 + \frac{d}{dt}\right)e^{-i\varphi}W(t+\tau).$$

Since $\varphi_\tau^\dagger\varphi_\tau = \mathbb{I}$, φ_τ is a unitary operator, which explains the purely imaginary spectrum of Fig. 1(b). Consequently, the inverse operator φ_τ^{-1}, that corresponds to backward time integration, is $\varphi_\tau^{-1} = \varphi_\tau^\dagger$.

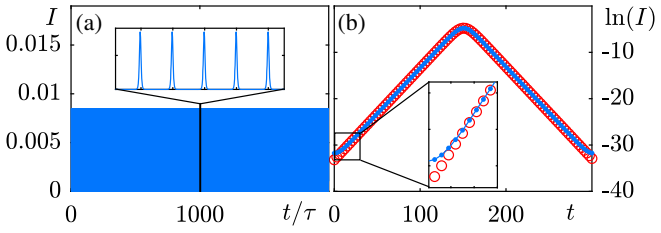

FIG. 2. (a) Temporal trace obtained by numerically integrating Eqs. (1) and (2) for $\tau = 300$. The period of the solution is $T = 301.5$ and the inset presents an enlarged view over five round-trips. The energy of the pulses is $\mu = 0.0063$. (b) Comparison between the profile of a single pulse of (a) (blue dots) and the analytical solution of the NLS equation (red circles) on a logarithmic scale. The only discrepancy can be seen at the interval boundaries (see inset).

Remarkably, the nonlinear equations (1) and (2) possess, in the long delay limit $\tau \gg 1$, periodic orbits with period $T = \tau + \Delta$ and $\Delta > 0$ [41] that correspond to solitary wave trains, see Fig. 2(a). The temporal profile of a single pulse coincides extremely well, even on a logarithmic scale, with a hyperbolic secant, a typical solution of the NLS equation [2], see Fig. 2(b). The small discrepancy at the tails is due to the fact that solitary solutions in time delayed dynamical systems are periodic orbits, which imposes a smooth reconnection of the solution with itself. An identical discrepancy would be observed if the NLS equation was solved over a periodic domain.

The link between the NDDE (6) and the NLS equation can be clarified by performing a multiscale analysis up to third order or using the functional mapping method [31,33]. We introduce the two time representation [14,15] by defining $\sigma \in [0, \tau]$ and $\theta \in \mathbb{N}$ so that time can be expressed as $t[\sigma, \theta] = \sigma + \theta\tau$. Assuming a field with carrier frequency δ as $E(t) = A(t)\exp(i\delta t)$ one obtains the following amplitude equation:

$$i(\partial_\theta + v\partial_\sigma)A + \tilde{\varphi}A - \frac{\beta_2}{2}\partial_\sigma^2 A - i\frac{\beta_3}{6}\partial_\sigma^3 A + \gamma|A|^2 A = 0, \tag{7}$$

that is, the NLS equation with third order dispersion with $v = 2/(1+\delta^2)$, $\beta_2 = 4\delta/(1+\delta^2)^2$, $\beta_3 = 4(3\delta^2 - 1)/(1+\delta^2)^3$ and $\gamma = 2/(1+\delta^2)$. The effective round-trip phase is $\tilde{\varphi} = \varphi - \delta\tau - 2\arctan(\delta) \bmod (2\pi)$. The second order dispersion coefficient β_2 cancels at resonance $\delta = 0$, which corresponds to the transition from anomalous to normal dispersion while third order dispersion β_3 vanishes for $\delta = \pm\delta_c$ where $\delta_c = 1/\sqrt{3}$. In this case Eq. (7) is equivalent to the classical NLS equation up to fourth order. In the anomalous dispersion regime where $\delta = -\delta_c$, $\beta_2 < 0$, $\gamma > 0$, and $\beta_3 = 0$, we obtain the so-called bright hyperbolic secant solitons [2]. The latter can be expressed as a one parameter family

$$A(\sigma, \theta; \mu) = \sqrt{\frac{2\mu}{\gamma}}\frac{\exp[i(\mu + \tilde{\varphi})\theta]}{\cosh[\sqrt{\frac{2\mu}{|\beta_2|}}(\sigma - v\theta)]}, \tag{8}$$

where we defined μ as the soliton energy, which together with the effective round-trip phase $\tilde{\varphi}$ contributes to the soliton frequency shift. The expression in Eq. (8) was given as an initial condition with parameters $(\mu, \varphi) = (0.005, 0)$, times a carrier frequency $\exp(-i\delta_c\sigma)$, to the periodic orbit solver of DDEBIFTOOL [42] which, after Newton iterations, converged to the periodic orbit shown in Fig. 2. The superposition in Fig. 2(b) using Eq. (8) was obtained without fit. In the normal dispersion regime, dark solitons, kink, and antikinks can be obtained similarly.

The existence of a unitary, hence reversible, differential operator for small amplitude solutions as well as the normal form (7) leading to the NLS equation indicates that Eq. (6) may possess a more general symmetry. In particular, one observes that Eq. (6) relates the field one step in the future $E_+(t)$ to the initial condition $\phi(t)$ as

$$E_+ + \dot{E}_+ - i|E_+|^2 E_+ = (\phi - \dot{\phi} + i|\phi|^2\phi)e^{i\varphi}. \tag{9}$$

Exchanging the left and right hand sides of Eq. (6) defines the field one step in the past E_- as

$$E_- - \dot{E}_- + i|E_-|^2 E_- = (\phi + \dot{\phi} - i|\phi|^2\phi)e^{-i\varphi}. \tag{10}$$

Following [43] we denote the nonlinear evolution operator over a step as Φ_τ and the mirror-conjugating involution R defined as $R[E(t)] = E^\star(-t)$. Reversibility is demonstrated since $R\circ\Phi_\tau\circ R^{-1} = \Phi_{-\tau}$, i.e., performing one step backward in time with the initial condition $\phi(t)$ is equivalent to one step forward for another initial condition $\phi^\star(-t)$ while mirror conjugating the end result, i.e., $E_+(t) = E_-^\star(-t)$. A demonstration of this property is depicted in Fig. 3(a). Starting from a complex, nonsolitonic initial condition we

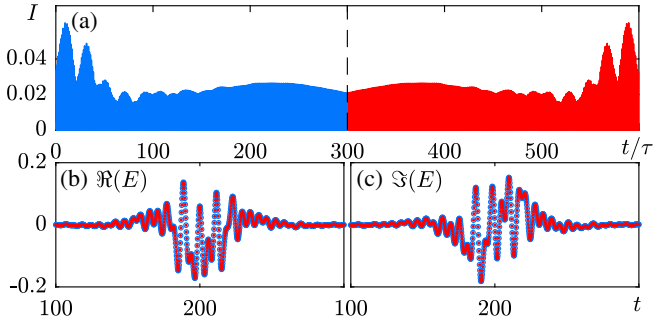

FIG. 3. (a) Numerical simulation showing the reversibility of Eq. (6). An asymmetric initial condition [blue circles in (b),(c)] is propagated 300 steps (blue part). Next, at the black dashed line in (a), the operator R is applied. After 300 steps (red part), the final profile shown in (b),(c) with red dots perfectly matches the initial condition after applying R a second time.

integrate Eq. (6) forward 300 steps, see Fig. 3(a). Then the operator R is applied to the resulting field profile. Further forward integration over 300 steps followed by the application of $R^{-1} = R$ leads to the perfect superposition with the initial condition shown in Figs. 3(b) and 3(c). We note that the mirror-conjugate symmetry is present in the NLS equation (7); it consists of setting $A(\sigma, \theta) \to A^{\star}(-\sigma, -\theta)$. We emphasize that, while the NLS equation is only an approximation of Eq. (6), the time reversal symmetry of Eq. (6) is an exact property.

The higher order terms that were neglected in deriving Eq. (7) scale as $\mathcal{O}(\mu^2)$. As such, Eq. (6) is only *integrable* for sufficiently small amplitude and smooth solutions. In this regime, we launched two solitons of equal amplitudes but slightly different carrier frequencies; this leads to different drift velocities thereby allowing for collisions. We notice that the in-phase (Figs. 4(a) and 4(b)) and the antiphase (Figs. 4(c) and 4(d)) solitons reproduce exactly the elastic behavior expected from an integrable equation [2].

Finally, we turn our attention to the existence of conserved quantities. Using Eq. (1) to write the equation for $|E|^2$ and combining Eq. (2) allows us to identify a discrete conserved quantity defined at each round-trip by

$$Q_\theta = 2\int_0^\tau |Y_\theta(\sigma)|^2 d\sigma + |E_\theta(0)|^2. \tag{11}$$

We interpret Q_θ as the soliton mass that contains the integral of the field intensity in the external cavity $|Y_\theta|^2$, while $|E_\theta(0)|^2$ is the intracavity field value. When the cavity snapshot is taken at a particular step θ, the pulse energy can either reside in the external cavity and be contained in the Y field, but it can also lay within the microcavity field E. We clarify the role of the conserved quantity in Fig. 5. The left panels (a),(c) depict the smooth evolution of a single soliton in the (σ, θ) representation.

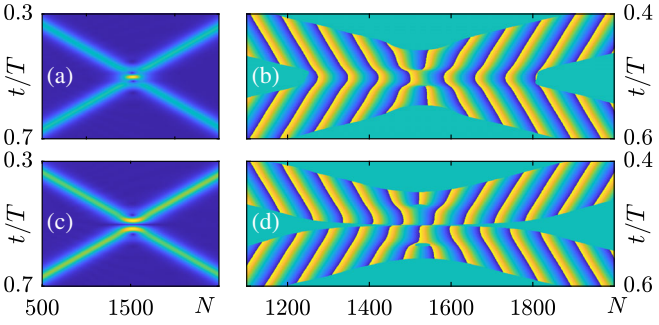

FIG. 4. Two-time representation of two colliding solitons of Eqs. (1) and (2) in-phase (a),(b) and antiphase (c),(d) as a function of the number of steps N. Panels (a) and (c) show the absolute value of the profile while (b) and (d) show their phase. Each pulse has an energy of $\mu = 0.005$ and $\delta_{1,2} = -\delta_c \pm 0.1$ while $\varphi = 1.95$. The mean carrier frequency $e^{-i\delta_c t}$ was factored out for clarity in (b),(d).

We notice that the nominal soliton mass in the NLS equation $q_\theta = \int^\tau |E_\theta|^2 d\sigma$ (black) is conserved up to the point where the soliton exits at $\sigma = \tau$ and reenters at $\sigma = 0$ at round-trip $\theta \simeq 130$. We notice that $\int^\tau |Y_\theta|^2 d\sigma$ also shows a downward kink, however, as $|E_\theta(0)|^2$ has an opposed spike, Q_θ is conserved. For a more complex initial condition with higher energy, one can observe a quick decomposition into multiple spikes after $\theta \simeq 40$ steps, cf. Fig. 5(b). Here, and even if the field remains well localized within the time delay until $\theta \simeq 120$ one already notices that q_θ is not conserved anymore, cf. Fig. 5(d). This high amplitude transient with fast temporal variations breaks the multiscale analysis leading to Eq. (7) and the high order terms like, e.g., self-steepening, result in a nonintegrable normal form. Yet, Q_θ still remains conserved in this case, too.

We conclude our analysis by performing the link between Eqs. (1) and (2) and a paradigm of dissipative pattern formation that is the Lugiato-Lefever equation [44]. The latter can be understood as a dissipative version of the NLS equation in which the phase symmetry is broken by the presence of monochromatic injection with amplitude Y_0 and frequency offset δ with respect to the microcavity resonance. In order to introduce this forcing, the external cavity should be open and one has to simultaneously introduce cavity losses by setting $r_e < 1$. This amounts to adding to the right hand side of Eq. (2) a term $Y_0\sqrt{1-r_e^2}$, see [40]. A similar multiscale analysis performed for small cavity losses and weak injection yields the Lugiato-Lefever equation with third-order dispersion

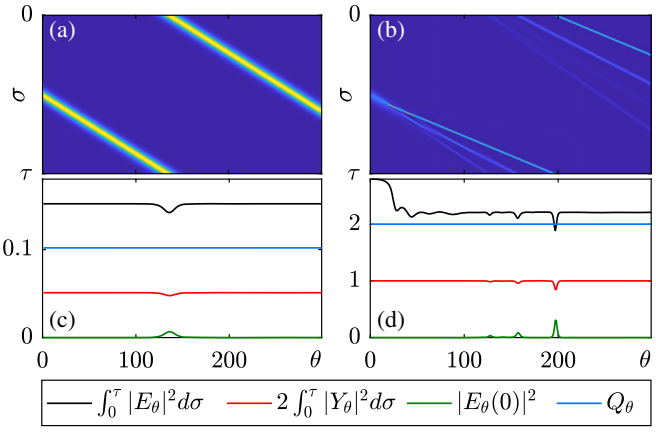

FIG. 5. (a),(b) Evolution of Eqs. (1) and (2) for different initial conditions. Note that the folding factor for these plots is τ, instead of T as in Fig. (4), leading to the drift of the soliton. The initial conditions are (a) a hyperbolic secant (8) with $\mu = 0.005$ and (b) a condition which is far away from a steady state. (c),(d) Evolution of different measures to visualize the conservation properties. In (c) all quantities are conserved unless the pulse reaches the edge of the cavity. Then only Q_θ is conserved. (d) The norm $\int_0^\tau |E_\theta|^2 d\sigma$ is not conserved and $2\int_0^\tau |Y_\theta|^2 d\sigma$ as well as $|E_\theta(0)|^2$ show the same imperfections when a soliton exits the cavity. However, Q_θ is conserved.

$$\left(i\partial_\theta+\tilde{\varphi}+i\upsilon\partial_\sigma-\frac{\beta_2}{2}\partial_\sigma^2-i\frac{\beta_3}{6}\partial_\sigma^3+\gamma|A|^2\right)A=F(A), \quad (12)$$

where $F(A)=i(r_e-1)A+iY_0\sqrt{8(1-r_e)}/(1+i\delta)$ contains both the effects of losses and injection.

In conclusion, we have demonstrated that nonlinear reversible TDSs exist and that they can host conservative solitons in the long delay limit, thereby bridging the gap with the results known for dissipative TDSs. The essential structure consists of a bilateral NDDE with an imaginary cubic nonlinearity which preserves the solution smoothness upon forward and backward propagation and may generate a unitary spectrum. The normal form identifies with the nonlinear Schrödinger equation, thereby allowing for bright and dark solitons although the lack of integrability can be observed at high energies. We believe that bilateral NDDEs open an avenue for the potential realization of conservative nonlinear dynamics in TDSs, such as, e.g., the Fermi-Pasta-Ulam-Tsingou [45] recurrence or the observation of the Korteweg–de Vries solitons.

J. J. acknowledges financial support of the MINECO Project MOVELIGHT (PGC2018-099637-B-100 AEI/FEDER UE). T. G. S. thanks the foundation "Studienstiftung des deutschen Volkes" for financial support. We thank S. Yanchuck and F. Maucher for useful discussions.

[1] G. P. Agrawal, *Nonlinear Fiber Optics* (Springer, New York, 2000).
[2] N. N. Akhmediev and A. Ankiewicz, *Solitons: Nonlinear Pulses and Beams* (Chapman & Hall, London, 1997).
[3] C. S. Gardner, J. M. Greene, M. D. Kruskal, and R. M. Miura, Phys. Rev. Lett. **19**, 1095 (1967).
[4] V. E. Zakharov, J. Appl. Mech. Tech. Phys. **9**, 190 (1968).
[5] H. C. Yuen and B. M. Lake, Annu. Rev. Fluid Mech. **12**, 303 (1980).
[6] L. Khaykovich, F. Schreck, G. Ferrari, T. Bourdel, J. Cubizolles, L. D. Carr, Y. Castin, and C. Salomon, Science **296**, 1290 (2002).
[7] N. J. Zabusky and M. D. Kruskal, Phys. Rev. Lett. **15**, 240 (1965).
[8] V. E. Zakharov and S. V. Manakov, Theor. Math. Phys. **19**, 551 (1974).
[9] B. A. Malomed, Physica (Amsterdam) **29D**, 155 (1987).
[10] S. Fauve and O. Thual, Phys. Rev. Lett. **64**, 282 (1990).
[11] N. Akhmediev and A. Ankiewicz, *Dissipative Solitons*, Lecture Notes in Physics Vol. 661 (Springer, Berlin, Heidelberg, 2005).
[12] T. Erneux, J. Javaloyes, M. Wolfrum, and S. Yanchuk, Chaos **27**, 114201 (2017).
[13] S. Yanchuk and G. Giacomelli, J. Phys. A **50**, 103001 (2017).
[14] G. Giacomelli and A. Politi, Phys. Rev. Lett. **76**, 2686 (1996).
[15] F. Marino and G. Giacomelli, Phys. Rev. E **102**, 052217 (2020).
[16] S. Yanchuk and G. Giacomelli, Phys. Rev. Lett. **112**, 174103 (2014).
[17] M. Wolfrum and S. Yanchuk, Phys. Rev. Lett. **96**, 220201 (2006).
[18] G. Giacomelli, F. Marino, M. A. Zaks, and S. Yanchuk, Europhys. Lett. **99**, 58005 (2012).
[19] G. Giacomelli, F. Marino, M. A. Zaks, and S. Yanchuk, Phys. Rev. E **88**, 062920 (2013).
[20] L. Larger, B. Penkovsky, and Y. Maistrenko, Phys. Rev. Lett. **111**, 054103 (2013).
[21] F. Marino, G. Giacomelli, and S. Barland, Phys. Rev. Lett. **112**, 103901 (2014).
[22] M. Marconi, J. Javaloyes, S. Balle, and M. Giudici, Phys. Rev. Lett. **112**, 223901 (2014).
[23] M. Marconi, J. Javaloyes, S. Barland, S. Balle, and M. Giudici, Nat. Photonics **9**, 450 (2015).
[24] B. Garbin, J. Javaloyes, G. Tissoni, and S. Barland, Nat. Commun. **6**, 5915 (2015).
[25] C. Schelte, P. Camelin, M. Marconi, A. Garnache, G. Huyet, G. Beaudoin, I. Sagnes, M. Giudici, J. Javaloyes, and S. V. Gurevich, Phys. Rev. Lett. **123**, 043902 (2019).
[26] J. K. Hale, *Functional Differential Equations*, Analytic theory of differential equations (Springer, Berlin, Heidelberg, 1971).
[27] S. M. V. Lunel and D. V. Yakubovich, Integr. Equations Oper. Theor. **27**, 347 (1997).
[28] V. Kolmanovskii and A. Myshkis, *Applied Theory of Functional Differential Equations* (Springer Science & Business Media, 2012), Vol. 85.
[29] J. Mulet and S. Balle, IEEE J. Quantum Electron. **41**, 1148 (2005).
[30] M. Marconi, J. Javaloyes, S. Balle, and M. Giudici, IEEE J. Sel. Top. Quantum Electron. **21**, 85 (2015).
[31] C. Schelte, J. Javaloyes, and S. V. Gurevich, Opt. Lett. **43**, 2535 (2018).
[32] P. Camelin, C. Schelte, A. Verschelde, A. Garnache, G. Beaudoin, I. Sagnes, G. Huyet, J. Javaloyes, S. V. Gurevich, and M. Giudici, Opt. Lett. **43**, 5367 (2018).
[33] C. Schelte, D. Hessel, J. Javaloyes, and S. V. Gurevich, Phys. Rev. Applied **13**, 054050 (2020).
[34] D. Hessel, S. V. Gurevich, and J. Javaloyes, Opt. Lett. **46**, 2557 (2021).
[35] R. Lang and K. Kobayashi, IEEE J. Quantum Electron. **16**, 347 (1980).
[36] F. Gires and P. Tournois, C.R. Hebd. Seances Acad. Sci. **258**, 6112 (1964).
[37] S. Yanchuk, L. Lücken, M. Wolfrum, and A. Mielke, Discrete Contin. Dyn. Syst. **35**, 537 (2015).
[38] For example, in the case of weak feedback $r_e \ll 1$, one could neglect the last term of Eq. (2) that is $\mathcal{O}(r_e^2)$.
[39] J. Mulet and S. Balle, IEEE J. Quantum Electron. **38**, 291 (2002).
[40] C. Schelte, A. Pimenov, A. G. Vladimirov, J. Javaloyes, and S. V. Gurevich, Opt. Lett. **44**, 4925 (2019).
[41] S. Yanchuk, S. Ruschel, J. Sieber, and M. Wolfrum, Phys. Rev. Lett. **123**, 053901 (2019).

[42] K. Engelborghs, T. Luzyanina, and D. Roose, ACM Trans. Math. Softw. **28**, 1 (2002).
[43] J. S. Lamb and J. A. Roberts, Physica (Amsterdam) **112D**, 1 (1998).
[44] L. A. Lugiato and R. Lefever, Phys. Rev. Lett. **58**, 2209 (1987).
[45] E. Fermi, J. Pasta, and S. M. Ulam, Studies of nonlinear problems. I, Technical Report No. LA-1940, 1955.